ISSN No:-2456-2165

Morphology Engineering toward High-Surface-Area Mno_2 Bifunctional Catalysts for Rechargeable Zinc-Air Batteries

Farwa[a], Israr Masood UI Hasan[a,c], Nengneng Xu[a, b]*, Jinli Qiao[a, b]*
[a]State Key Laboratory for Modification of Chemical Fibers and Polymer Materials, College of Environmental Science and Engineering, Donghua University, 2999 Ren'min North Road, Shanghai 201620, P. R. China
[b]Shanghai Institute of Pollution Control and Ecological Security, 1515 North Zhongshan Road, Shanghai 200092, China
[c]Institute of Soil and Environmental Sciences, University of Agriculture Faisalabad, Faisalabad,Pakistan

Abstract:- Rechargeable zinc-air battery showslow cost, high safety and high theoretical power/energydensity, which is one of the most promising energy technologies for future energy storage and power battery. Nevertheless, the energy efficiency is greatly limited by the slow kinetics of oxygen reduction reaction/oxygen evolution reaction (ORR/OER) on the cathode. In this work, different morphological MnO_2catalysts with high surface areas were synthesized by mild hydrothermal-calcined processes.Their morphology, crystal structure and specific surface areawere obtained and furtheranalyzed by SEM, XRD, nitrogen adsorption and desorptiontests.

The results show that the MnO_2 nanoparticles with 50 nm exhibits higher catalytic activitiesthanother morphological MnO_2 catalysts. In addition, the MnO_2 nanoparticleswith 50 nm shows higher power density (229 mW cm^{-2}) and more stable charge-discharge performance with low voltage drop (0.82 V for 100 h) than that of noble metal catalyst (Pt/C+ RuO_2). This work provides a new idea for the development and application of MnO_2-based bifunctional catalysts.

Keywords:- *Morphology engineering, MnO_2, bifunctional catalyst, zinc-air battery.*

I. INTRODUCTION

Along with the increasing demand of renewable energy and the continuous development of clean energy technology, zinc-air battery is considered as an excellent energy storage and conversion device on account of its low cost, high power density and admirable stability[1-2]. The core challenge of zinc-air battery is to explore efficient bifunctional catalysts to overcome the slow kinetics of oxygen evolution reaction (OER) and oxygen reduction reaction (ORR). Noble metalbased catalysts such as Pt/C and RuO_2 are commonly used commercial ORR and OER catalysts, respectively, and they displayed better catalytic performance than the pure metals and metal oxides[3-4].However, their scarcity and high pricemake the noble-metal based catalysts be inapplicable in practical scale applications. Accordingly, it is necessary to develop low-cost and efficient bifunctional catalysts, e.g. Mn-based catalysts,[5-7] Fe-based catalysts,[8-9]Co-based catalysts,[10]and certainperovskite catalysts[11-12] to replace the noble metal or their oxides based catalysts.

In practical applications, as a commercial non-noble metal cathode active material, MnO_2 is widely used in zinc-air batteries because of its low cost, simple preparation, low toxicity, environmentally friendly, and considerable performanceto ORR and OERin the alkalineelectrolytes.[13-15]In addition, the ultimate catalytic performance of MnO_2 have been considered to be affected by its intrinsic structure (e.g., crystalline phases, particle size, shape, and surface area, etc.). For example, the oxygen catalytic property of MnO_2 has been revealed tofollow the orders:$\alpha \sim \delta\text{–}MnO_2 > \gamma\text{–}MnO_2 > \lambda\text{–}MnO_2 > \beta\text{–}MnO_2$, $\alpha\text{–}MnO_2$>amorphous$MnO_2 > \beta\text{–}MnO_2 > \gamma\text{–}MnO_2$ or $\alpha\text{–}MnO_2$>amorphous$MnO_2 > \beta\text{–}MnO_2 > \delta\text{–}MnO_2$.[6, 16-17]According to the two sequences, fortunately,α-MnO_2showed the highest oxygen catalytic activity of all the crystal structures, which should be attributed to its large 2*2 tunnel structure.[18]Compared to other tunnel structures, the large 2*2 tunnel structure facilitate the active ion transfer within the lattice framework, thereby accelerating the ORR and OER rates. Besides, the surface of α-MnO_2 has been confirmed to be rich in hydroxyl groups and defects, which is conducive to improving the local environment for the key steps of the oxygen-catalyzed reaction (adsorption of oxygen molecules and breaking of oxygen double bonds).[19-20]In addition to the crystal structure, the morphology of α-$MnO_2$is also another key factor affecting its performance. According to literature, in terms of morphology, the sequence of its activity has been documented as follows: nanowires> nanotubes> nanoparticles. The structure and surface morphology of manganese dioxide have been studied a lot, and good progress has been made. However, for MnO_2 with the same crystal structure (such as α-MnO_2), there is still no accepted rule on the relationship between the morphology (specific surface area) and catalytic performance.

Herein,this work synthesized different morphological MnO_2catalysts by changing the reducing agent, further obtained different particle size by controlling the reaction time, aims to demonstrate the relationship between the morphology (specific surface area) and catalytic performance of α-MnO_2. As expected, its sequence as follows: nanoparticles>nanospindle>nanoblock>micro-sphere.For α-MnO_2nanoparticles, the larger the specific surface area, the higher the oxygen catalytic activity. The MnO_2 nanoparticles with 50 nm exhibits lower overpotential of 0.825 V than other morphological MnO_2 catalysts, and

shows higher power density (229 mW cm^{-2}) and longer charge-discharge durability (100 h) than that of noble metal catalyst (Pt/C+ RuO_2).

II. EXPERIMETAL SECTION

A. Preparation of materials:

- **Synthesis of α-MnO_2 with different morphologies.**0.79g potassium permanganate as raw materials and oxidants (purity >99.5%, Macklin Chemical Reagent Co., Ltd.) was weighed and dissolved in50 mL of deionized (D.I.) water. Then, 0.20 g citric acid(purity>99.5%, Macklin Chemical Reagent Co., Ltd.) was added into the above solution. The final solution was quickly transferred into a steel autoclave kept at 140 °C for 4 hours. As the temperature of the steel autoclave drops to room temperature, the precursor powder was obtained bycentrifugal washing with water and ethanol for 3 times respectively. The precursor sample was then dried in an oven at 60°C for 24 hours, then ground and calcined in a Muffle oven at 350° for 1 hour. The and was annealed in a furnace at 350 °C for 1 h. These final solid powder sample was collected and denoted asα-$MnO_{2\text{-ca}}$. In addition, under the condition of maintaining other reaction conditions, these powder samples with different morphologies can be obtained by replacing citric acid with glucose, urea and ethanol respectively, which further denoted asα-$MnO_{2\text{-gl}}$, α-$MnO_{2\text{-ur}}$, and α-$MnO_{2\text{-et}}$, respectively. To further study the particle size, changing the hydrothermal reaction time of α-$MnO_{2\text{-et}}$ were carried out. Specifically, the final solutions with ethanol were quickly transferred into a steel autoclave kept at 140 °C for 2 hours and 6 hours, respectively (denoted as α-$MnO_{2\text{-et-2h}}$ and α–$MnO_{2\text{-et-4h}}$).

B. Materials characterizations:

The microstructure of the samples was characterized by field emission scanning electron microscopy (FE-SEM, FEI Sirion 200). The specific surface area of the samples was determined by Autosorb-iQ automatic area and aperture analyzer. The crystal structure was determined by X-ray diffraction (XRD) (D/MAX-2550 PC).

C. Electrochemical measurement:

First, 4mg of the above samples and 1mg of carbon nanotubes were added to the mixed solution of 1ml ethanol and 16ml 5% Nafion, followed by ultrasound for 30min to prepare sample ink. The sample ink of 9.8 µl was dropped on the black glass carbon surface of the rotating disk electrode (RDE, area: 0.19625 cm^{-2}) with pipettes and dried into a homogeneous catalytic film (the loadingof active materials: 200 µg cm^{-2}).The oxygen catalyticactivities of samples wereperformed by CHI760D electrochemical workstation in the conventional half-cell system. Thehalf-cell system consists of counter electrode (Ptt mesh), reference electrode (saturated calomel electrode,SCE) and working electrode (rotating disk electrode, RDE).The ORR and OER performance wereevaluated by linear sweep voltammetry (LSV, scan rate of 5 mV s^{-1}) at 1600 rpm in O_2-saturated 0.1 M KOH solution. All potentials of the obtained LSV curveswere converted to reversible hydrogen electrode (RHE)on the basis of the following equation:

$$E(vs.RHE) = E(vs.SCE) + 0.059 \times pH + 0.241\ V \quad \textbf{(1)}$$

Notably, the reference catalyst sample was a mixture of commercial Pt/C (20 wt%, Johnson Matthey) and RuO_2 (Xian Kaili Co., Ltd.).

D. Rechargeable zinc-air batteries assembly:

Similarly, 10mg of the above samples and 2mg of carbon nanotubes were added to the mixed solution of 9.9 ml ethanol and 100 µl 5% Nafion, followed by ultrasound for 30min to prepare sample slurry. The prepared slurry was sprayed on the surface of the gas diffusion layer (GDL) at 70°C to obtain an air electrode. Then, the zinc sheet (thickness: 0.3mm, aera: 9 cm^2)and the obtained air electrode (active aera: 4 cm^2, loading:1 $mgcm^{-2}$) are respectively placed in the home-made fixture to assemble the zinc air battery. 6 M KOH solution was used as the electrolyte. The discharging polarization curve of sample is obtained by LSV. The charge-discharge cycle performance of the battery is evaluated by constant current pulse (current density: 10 mA cm^{-2}, individual cycle time: 10 mins).

III. RESULT AND DISCUSSION

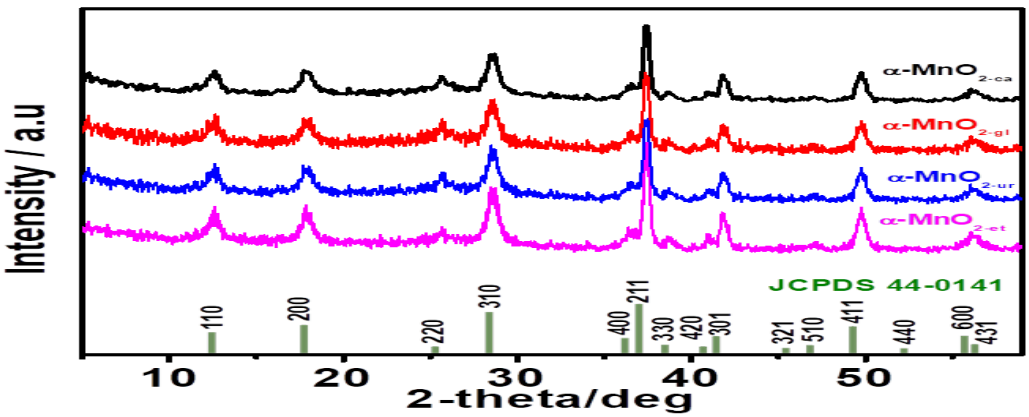

Fig. 1: The XRD patterns ofα–$MnO_{2\text{-ca}}$, α-$MnO_{2\text{-gl}}$, α–$MnO_{2\text{-ur}}$ and α-$MnO_{2\text{-et}}$

ISSN No:-2456-2165

- **Physical characterization.**The crystal structure ofMnO2 prepared using different reducing agents (α-MnO2-ca, α-MnO2-gl, α-MnO2-ur and α-MnO2-et) was obtained by performing XRD. As shown in Fig. 1, the characteristic peaks of all samples are close and consistent with the standard cards (JCPDS 44e0141), means that all samples synthesized using different reducing agents areα-MnO2.The characteristic peaks ofα-MnO2-ca, α-MnO2-gl, α-MnO2-ur and α-MnO2-etat 12.8°, 18.1°, 25.7°, 28.8°,36.7°, 39.1°41.2°, 41.9°, 46.1°, 47.3°, 49.9°, 52.9°, 56.3° and 56.9° correspond to the(110), (200), (220), (310), (400), (211), (330), (420), (301), (321), (510), (411), (440), (600) and (431) planes of α-MnO2.In addition, the morphology and structure of these samples were further obtained by SEM (Fig.2). As shown in Fig. 2a, α-MnO2-ca prepared with citric acid showed a unique arbutus-like spherical morphology, and the particle size was about 3-4μm. Notably,the surface of α-MnO2-ca, similar to arbutus, consists of a rich aggregation of nanorods.In addition, α-MnO2-gl prepared with glucose showed two different morphologies: "spindle (1.5-2 μm)" and "cube (1.5 μm)".Both have relatively dense surfaces. While urea was used as the reducing agent, α-MnO2-urexhibits irregular morphology formed by the accumulation of massive block units with different nanometer sizes (50-100 nm). Similar to α-MnO2-ur, α-MnO2-et also exhibits irregular morphology. However, the irregular morphology is caused by the aggregation of nanometer spherical particles. Interestingly, the spherical particles are all around 50 nanometers in size.

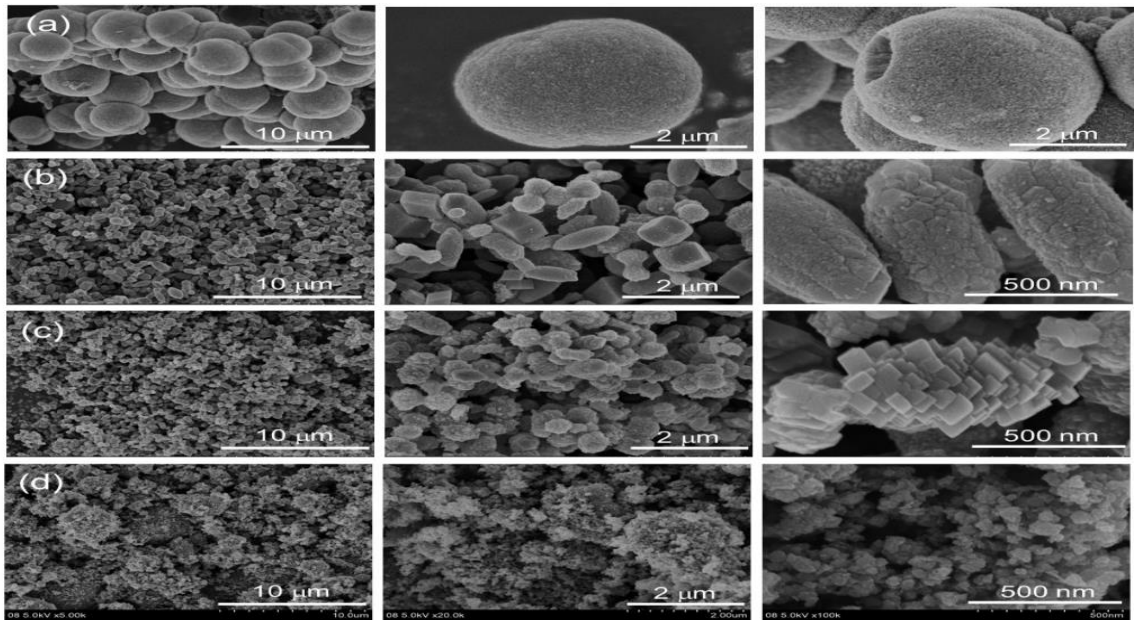

Fig. 2: SEM images under different resolutions(a)α-$MnO_{2\text{-}ca}$, (b) α-$MnO_{2\text{-}gl}$, (c)α-$MnO_{2\text{-}ur}$ and (d) α-$MnO_{2\text{-}et}$

In general, the surface area of a catalyst is affected by its morphology. The specific surface area directly determines the exposure probability of the active site. To this end, the specific surface area was obtained by testing the nitrogen adsorption/desorption isotherm of the sample (Fig. 3). The Brunauer-Emmett-Teller (BET) specific surface areas of α-$MnO_{2\text{-}ca}$, α-$MnO_{2\text{-}gl}$, α-$MnO_{2\text{-}ur}$ and □-$MnO_{2\text{-}et}$are 15.1 m^2 g^{-1}, 32.4 m^2 g^{-1}, 37.2 m^2 g^{-1}, 45.3 m^2 g^{-1}, respectively. This phenomenon indicated that MnO_2 prepared with ethanol as reducing agent (α-$MnO_{2\text{-}et}$) exhibited the highest specific surface area. In addition, the results correspond to the particle size of samples from SEM images. There is no doubt that the high specific surface of the catalyst can not only effectively provide abundant active sites, but also improve the mass transfer and accommodate more electrolyte to accelerate ion transfer, thus contributing to the improvement of ORR and OER activity.

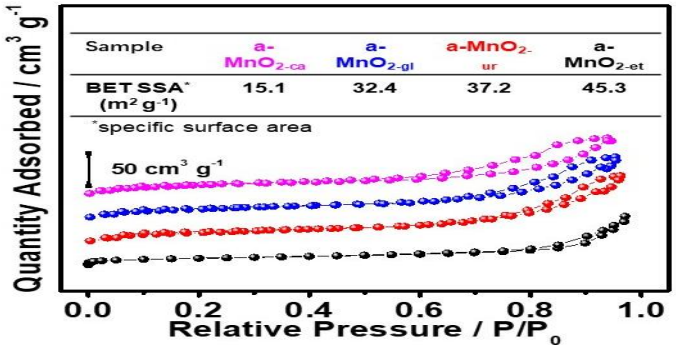

Fig. 3: N_2adsorption/desorption isotherms and inset table: the corresponding surface areas of α-$MnO_{2\text{-}ca}$, α-$MnO_{2\text{-}gl}$, α-$MnO_{2\text{-}ur}$ and α-$MnO_{2\text{-}et}$.

ISSN No:-2456-2165

- **Electrochemical performance**. In order to evaluate their ORR/OER activity, LSV was performed in O_2-saturated aqueous solution (0.1 M KOH). As shown in Fig. 4a, the half-wave potential ($E_{1/2}$) of α-$MnO_{2\text{-}et}$is 0.836 V, which is more positive than α-$MnO_{2\text{-}ca}$ (0.780 V), α-$MnO_{2\text{-}gl}$(0.712 V) and α-$MnO_{2\text{-}ur}$ (0.811), and which is close to Pt/C+RuO_2 (0.864 V). It is worth noting thatα-$MnO_{2\text{-}et}$ has the highest limiting current

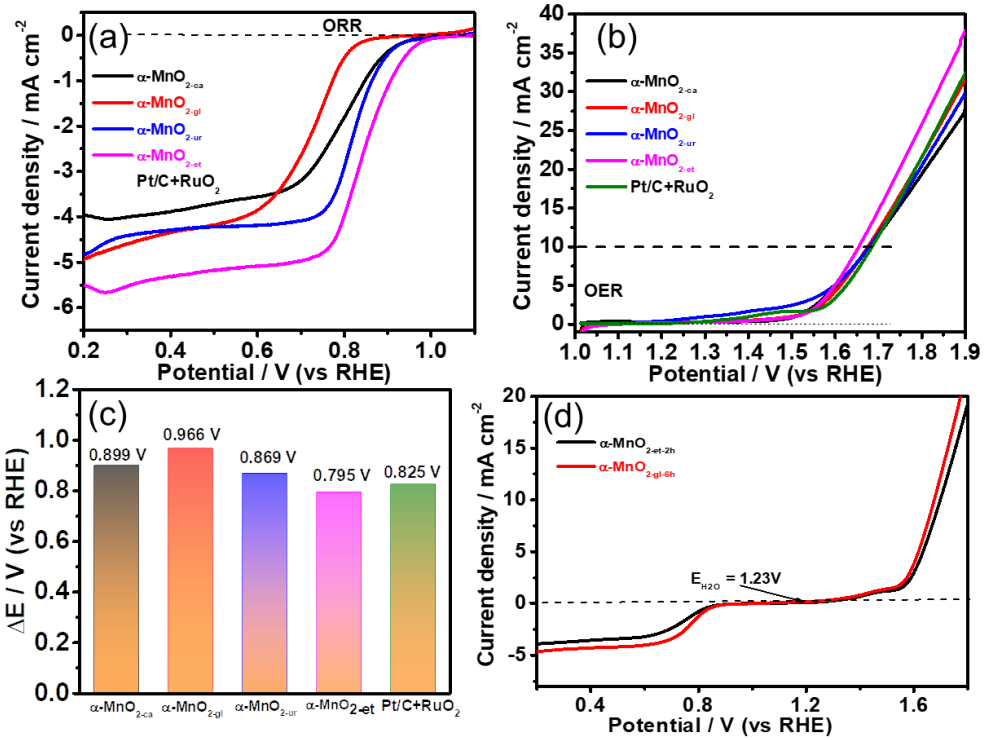

Fig. 4: (a) ORR curves ofα-$MnO_{2\text{-}ca}$, α-$MnO_{2\text{-}gl}$, α-$MnO_{2\text{-}ur}$, α-$MnO_{2\text{-}et}$, and Pt/C+RuO_2, (b) OER curves ofα-$MnO_{2\text{-}ca}$, α-$MnO_{2\text{-}gl}$, α-$MnO_{2\text{-}ur}$, α-$MnO_{2\text{-}et}$, and Pt/C+RuO_2, (c) ΔE of α-$MnO_{2\text{-}ca}$, α-$MnO_{2\text{-}gl}$, α-$MnO_{2\text{-}ur}$, α-$MnO_{2\text{-}et}$, and Pt/C+RuO_2, and (d) ORR-OER curves of α-$MnO_{2\text{-}et\text{-}2h}$ and α-$MnO_{2\text{-}et\text{-}6h}$.

density of 5.5 mA cm^{-2} among all tested samples, indicating that nanoparticle MnO_2 has a faster mass transfer rate than other morphologies. In addition to ORR activity, OER activity is also a key index for performance evaluation of bifunctional catalysts.Similarly to ORR activity, α-$MnO_{2\text{-}et}$ also exhibited the lowest overpotential at 10 mA cm^{-2} (400 mV) and the highest current density of 37 mA cm^{-2} at 1.9 V at in all samples to be measured, including the precious metal catalyst (Fig. 4b).To facilitate the assessment of overall catalyst activity, the gap(ΔE) between the $E_{1/2}$ and E_{10} (potential at 10 mA cm^{-2}) arecalculated (Fig. 4c). The smaller the gapvalue, the closer the sample is to the ideal bifunctional catalyst.By this index, the ΔEof α-$MnO_{2\text{-}et}$ is 0.825 V, which is better than that of other morphologies of MnO_2 (α-$MnO_{2\text{-}ca}$:0.899 V, α-$MnO_{2\text{-}gl}$: 0.966 V, andα-$MnO_{2\text{-}ur}$: 0.869 V) and Pt/C+RuO_2(0.825 V), demonstrating that nanoparticle α-$MnO_{2\text{-}et}$ is apromising reversible oxygen electrode. Combined with SEM and specific surface area data, the oxygen catalytic property of $MnO_2$is revealed to follow the sequence: α-$MnO_{2\text{-}et}$ (nanospherical particle, 45.3 m^2 g^{-1}) >α-$MnO_{2\text{-}ur}$ (nano block, 37.2 m^2 g^{-1}) >α-$MnO_{2\text{-}ca}$ (arbutus-likemicrosphere,15.1 m^2 g^{-1}) > α-$MnO_{2\text{-}gl}$ (spindle andcube,32.4 m^2 g^{-1}). Paradoxically, the surface area of α-$MnO_{2\text{-}gl}$is higher than that of α-$MnO_{2\text{-}ca}$, but the oxygen catalytic activity of α-$MnO_{2\text{-}gl}$is lower than that of α-$MnO_{2\text{-}ca}$.The main reason for this seeming anomaly may betheunique arbutus-like spherical morphology of α-$MnO_{2\text{-}ca}$.The loose surface structure is conducive to the adsorption and dissociation of oxygen /OH- ions. Whileα-$MnO_{2\text{-}gl}$shows a large specific surface area due to its small particle size, its dense surface inhibits the oxygen-catalyzed reaction.

ISSN No:-2456-2165

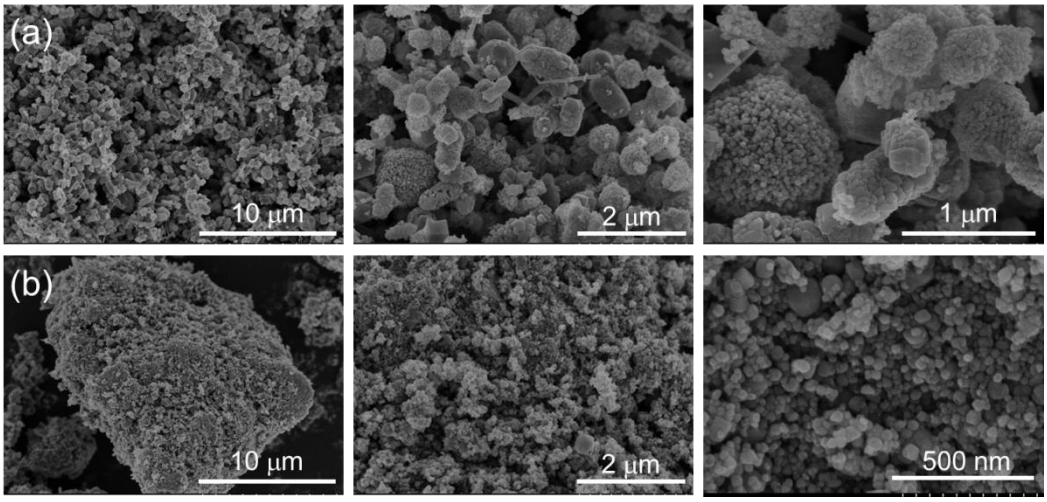

Fig. 5: SEM images under different resolutions(a)α-$MnO_{2\text{-}et\text{-}2h}$ and (b) α-$MnO_{2\text{-}et\text{-}6h}$

In addition, the nanoparticle α-$MnO_{2\text{-}et}$ shows better ORR and OER activities thanα-$MnO_{2\text{-}et\text{-}2h}$ and α-$MnO_{2\text{-}et\text{-}6h}$ (Fig. 5d).The finding reveals that 1) the short preparation time makes it difficult to form the active site of catalyst, which directly affects the performance of catalyst (Fig. 5b); and 2)the agglomeration of nanoparticles caused by longer preparation time will reduce the bifunctional activity of catalysts (Fig. 5b).

- **Performance of Zn-air batteries.** The practical battery performance is a key parameter for bifunctional catalysts. Thereby, we design a home-made rechargeable zinc-air battery fixture (rZAB) and its schematic diagram is displayed in Fig.6a.The power density and durability of a-$MnO_{2\text{-}et}$ and Pt/C+RuO_2 were obtained by rechargeable zinc air battery. As shown in Fig. 6b, the open-circuit voltage (OCV) of the a-$MnO_{2\text{-}et}$-based zinc-air battery is 1.54 V, which is higher than that of Pt/C+RuO_2 (1.48 V). In addition, the working voltages at 100 mA cm^{-2} of a-$MnO_{2\text{-}et}$-based and Pt/C+RuO_2-based zinc-air batteries are 1.1 V and 0.8 V, respectively. Notably, the a-$MnO_{2\text{-}et}$-based zinc-air battery shows higher power density with 229 mW cm^{-2} at 0.58 V than that of Pt/C+RuO_2 (91 mW cm^{-2}at 0.5 V) and some recently reported works.[15, 21-23] To sum up, the above results with higher OCV, high power density and higher discharge voltages demonstrate that a-$MnO_{2\text{-}et}$ possess excellent energy storage and release performance, showing great potential in primary zinc-air battery applications.

In a practical rechargeable battery, the long cycling durability is desired to achieve long life and is very core indicators. Thus, the charge-discharge cycles stability test at a constant current density was carried out (Fig. 6c). As shown in Fig. 4c, the a-$MnO_{2\text{-}et}$-based zinc-air battery shows initial discharging voltage of 1.30 V and charging voltage of 2.10 V at a current density of 10 mA cm^{-2}, with a small voltage gap of 0.8 V and a high voltage efficiency of 61.9%, which is superior to Pt/C+RuO_2 (initial discharging voltage: 1.05 V, charging voltage: 2.10 V, voltage gap: 0.8 V and voltage efficiency: 50.0%). Notably, after 26 h cycling, the Pt/C+RuO_2-based zinc-air battery shows an obvious voltage gap increase of 33.3%. In addition, the rising trend of voltage difference increases with the extension of stability test time. It wasn't until 60 hours later that the voltage difference peaked (~ 2 V). Fortunately, the a-$MnO_{2\text{-}et}$-based zinc-air battery maintains a stable voltage drop of 0.82 V throughout the test (100hours), which directly indicating its good oxygen catalytic durability.

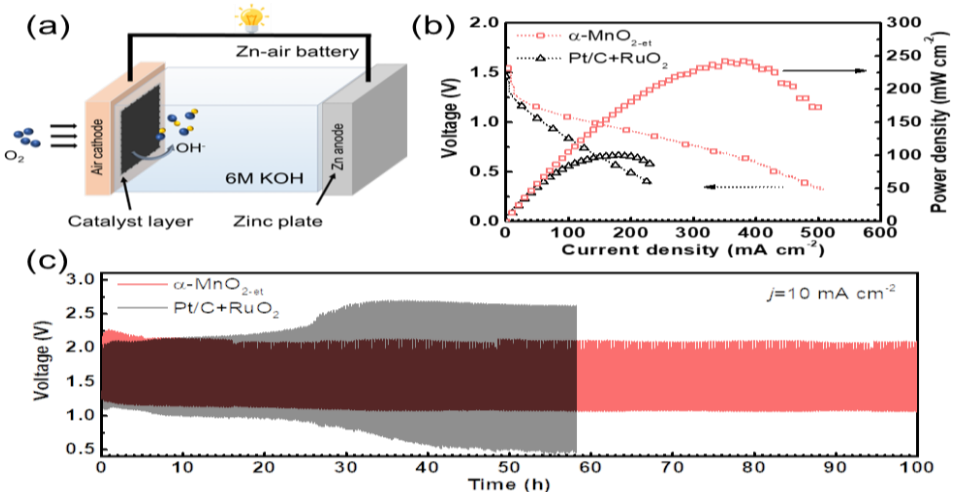

Fig. 6: (a) schematic diagram of home-made zinc-air battery, (b) polarization curves and its corresponding power density curves of a-$MnO_{2\text{-}et}$ and Pt/C+RuO_2, (c) charge-discharge curves at a current density of 10 mA cm^{-2} of a-$MnO_{2\text{-}et}$ and Pt/C+RuO_2.

ISSN No:-2456-2165

IV. CONCLUSIONS

In summary, the different morphological MnO2catalysts with different specific surface areas were synthesized by mild hydrothermal-calcined processes.α-MnO2-ca,α-MnO2-gl, α–MnO2-ur and α–MnO2-etshowed a unique arbutus-like microsphere, "spindle" and "cube" structure, nano block, and nano spherical particle, respectively. In addition, The BET specific surface areas of α–MnO2-ca, α–MnO2-gl, α–MnO2-ur and α-MnO2-etare 15.1 m2 g-1, 32.4 m2 g-1, 37.2 m2 g-1, 45.3 m2 g-1,respectively. As expected, the oxygen catalytic property of MnO2is revealed to follow the order: α–MnO2-et>α–MnO2-ur>α–MnO2-ca> α–MnO2-gl. Notably, α–MnO2-et showed good oxygen catalytic activity with low ΔE of 0.825 V, high OCV of 1.54 V, high power density of229 mW cm-2, and long-term discharge-charge cycle stability with low voltage gap of 0.8 V for 100 hours.This work provides a new idea for preparing high performance and low cost bifunctional manganese based catalysts.

ACKNOWLEDGMENTS

This work is financially supported by the “Scientific and Technical Innovation Action Plan” Hong Kong, Macao and Taiwan Science & Technology Cooperation Project of Shanghai Science and Technology Committee (19160760600), National Natural Science Foundation of China (21972017), the Fundamental Research Funds for the Central Universities (2232022D-18) and Shanghai Sailing Program (22YF1400700).

- **Competing interests:** The authors declare no competing financial interests.

REFERENCES

[1.] Xu, N.; Zhang, Y.; Wang, M.; Fan, X.; Zhang, T.; Peng, L.; Zhou, X.-D.; Qiao, J. High-performing rechargeable/flexible zinc-air batteries by coordinated hierarchical Bi-metallic electrocatalyst and heterostructure anion exchange membrane. *Nano Energy* 2019,*65*, DOI: 10.1016/j.nanoen.2019.104021.

[2.] Xu, N.; Zhang, Y.; Zhang, T.; Liu, Y.; Qiao, J. Efficient quantum dots anchored nanocomposite for highly active ORR/OER electrocatalyst of advanced metal-air batteries. *Nano Energy* 2019,*57*, 176-185, DOI: 10.1016/j.nanoen.2018.12.017.

[3.] Zhang, Y.; Deng, Y.-P.; Wang, J.; Jiang, Y.; Cui, G.; Shui, L.; Yu, A.; Wang, X.; Chen, Z. Recent Progress on Flexible Zn-Air Batteries. *Energy Storage Materials* 2021,*35*, 538-549, DOI: 10.1016/j.ensm.2020.09.008.

[4.] Yin, Z.; He, R.; Xue, H.; Chen, J.; Wang, Y.; Ye, X.; Xu, N.; Qiao, J.; Huang, H. A bimetallic-activated MnO₂ self-assembly electrode with a dual heterojunction structure for high-performance rechargeable zinc-air batteries. *Energy Materials* 2022,*2* (3), 200021, DOI: 10.20517/energymater.2022.17.

[5.] Jiang, H.; Dai, Y.; Hu, Y.; Chen, W.; Li, C. Nanostructured Ternary Nanocomposite of rGO/CNTs/MnO2 for High-Rate Supercapacitors. *ACS Sustainable Chemistry & Engineering* 2013,*2* (1), 70-74, DOI: 10.1021/sc400313y.

[6.] Xu, N.; Liu, J.; Qiao, J.; Huang, H.; Zhou, X.-D. Interweaving between MnO2 nanowires/ nanorods and carbon nanotubes as robust multifunctional electrode for both liquid and flexible electrochemical energy devices. *J. Power Sources* 2020,*455*, 227992, DOI: 10.1016/j.jpowsour.2020.227992.

[7.] Gorlin, Y.; Jaramillo, T. F. A Bifunctional Nonprecious Metal Catalyst for Oxygen Reduction and Water Oxidation. *J. Am. Chem. Soc.* 2010,*132* (39), 13612-13614, DOI: 10.1021/ja104587v.

[8.] Wang, C.; Li, Z.; Wang, L.; Niu, X.; Wang, S. Facile Synthesis of 3D Fe/N Codoped Mesoporous Graphene as Efficient Bifunctional Oxygen Electrocatalysts for Rechargeable Zn–Air Batteries. *ACS Sustainable Chemistry & Engineering* 2019,*7* (16), 13873-13885, DOI: 10.1021/acssuschemeng.9b02052.

[9.] Qiao, Y.; Yuan, P.; Hu, Y.; Zhang, J.; Mu, S.; Zhou, J.; Li, H.; Xia, H.; He, J.; Xu, Q. Sulfuration of an Fe–N–C Catalyst Containing FexC/Fe Species to Enhance the Catalysis of Oxygen Reduction in Acidic Media and for Use in Flexible Zn–Air Batteries. *Adv. Mater.* 2018,*30* (46), 1804504, DOI: 10.1002/adma.201804504.

[10.] Chen, S.; Ma, L.; Wu, S.; Wang, S.; Li, Z.; Emmanuel, A. A.; Huqe, M. R.; Zhi, C.; Zapien, J. A. Uniform Virus-Like Co–N–Cs Electrocatalyst Derived from Prussian Blue Analog for Stretchable Fiber-Shaped Zn–Air Batteries. *Adv. Funct. Mater.* 2020,*30* (10), 1908945, DOI: 10.1002/adfm.201908945.

[11.] Han, X.; Cheng, F.; Zhang, T.; Yang, J.; Hu, Y.; Chen, J. Hydrogenated Uniform Pt Clusters Supported on Porous CaMnO3 as a Bifunctional Electrocatalyst for Enhanced Oxygen Reduction and Evolution. *Adv. Mater.* 2014,*26* (13), 2047-2051, DOI: 10.1002/adma.201304867.

[12.] Wang, Z.; Zhang, F.; Jin, C.; Luo, Y.; Sui, J.; Gong, H.; Yang, R. La 2 O 3 -NCNTs hybrids in-situ derived from LaNi 0.9 Fe 0.1 O 3 -C composites as novel robust bifunctional oxygen electrocatalysts. *Carbon* 2017,*115*, 261-270, DOI: 10.1016/j.carbon.2017.01.016.

[13.] Wang, Y.-J.; Fang, B.; Zhang, D.; Li, A.; Wilkinson, D. P.; Ignaszak, A.; Zhang, L.; Zhang, J. A Review of Carbon-Composited Materials as Air-Electrode Bifunctional Electrocatalysts for Metal–Air Batteries. *Electrochemical Energy Reviews* 2018,*1* (1), 1-34, DOI: 10.1007/s41918-018-0002-3.

[14.] Ding, J.; Ji, S.; Wang, H.; Brett, D. J. L.; Pollet, B. G.; Wang, R. MnO/N-Doped Mesoporous Carbon as Advanced Oxygen Reduction Reaction Electrocatalyst for Zinc-Air Batteries. *Chemistry* 2019,*25* (11), 2868-2876, DOI: 10.1002/chem.201806115.

[15.] Zhang, T.; Li, Z.; Sun, P.; Wang, L.; Niu, X.; Wang, S. α-MnO2 nanorods supported on three dimensional

graphene as high activity and durability cathode electrocatalysts for magnesium-air fuel cells. *Catal. Today* 2019, DOI: 10.1016/j.cattod.2019.04.055.

[16.] Li, P.-C.; Hu, C.-C.; Lee, T.-C.; Chang, W.-S.; Wang, T. H. Synthesis and characterization of carbon black/manganese oxide air cathodes for zinc-air batteries. *J. Power Sources* 2014,*269*, 88-97, DOI: 10.1016/j.jpowsour.2014.06.108.

[17.] Lee, D. U.; Xu, P.; Cano, Z. P.; Kashkooli, A. G.; Park, M. G.; Chen, Z. Recent progress and perspectives on bi-functional oxygen electrocatalysts for advanced rechargeable metal–air batteries. *Journal of Materials Chemistry A* 2016,*4* (19), 7107-7134, DOI: 10.1039/c6ta00173d.

[18.] Xu, N.; Nie, Q.; Luo, L.; Yao, C.; Gong, Q.; Liu, Y.; Zhou, X.-D.; Qiao, J. Controllable Hortensia-like MnO2 Synergized with Carbon Nanotubes as an Efficient Electrocatalyst for Long-Term Metal–Air Batteries. *ACS applied materials & interfaces* 2019,*11* (1), 578-587, DOI: 10.1021/acsami.8b15047.

[19.] Lee, S.; Nam, G.; Sun, J.; Lee, J. S.; Lee, H. W.; Chen, W.; Cho, J.; Cui, Y. Enhanced Intrinsic Catalytic Activity of lambda-MnO2 by Electrochemical Tuning and Oxygen Vacancy Generation. *Angew. Chem. Int. Ed. Engl.* 2016,*55* (30), 8599-604, DOI: 10.1002/anie.201602851.

[20.] Xu, N.; Zhang, Y.; Wang, M.; Fan, X.; Zhang, T.; Peng, L.; Zhou, X.-D.; Qiao, J. High-performing rechargeable/flexible zinc-air batteries by coordinated hierarchical Bi-metallic electrocatalyst and heterostructure anion exchange membrane. *Nano Energy* 2019,*65*, 104021, DOI: 10.1016/j.nanoen.2019.104021.

[21.] Ma, L.; Chen, S.; Pei, Z.; Huang, Y.; Liang, G.; Mo, F.; Yang, Q.; Su, J.; Gao, Y.; Zapien, J. A.; Zhi, C. Single-Site Active Iron-Based Bifunctional Oxygen Catalyst for a Compressible and Rechargeable Zinc-Air Battery. *ACS Nano* 2018,*12* (2), 1949-1958, DOI: 10.1021/acsnano.7b09064.

[22.] Wang, M.; Lai, Y.; Fang, J.; Qin, F.; Zhang, Z.; Li, J.; Zhang, K. Hydrangea-like NiCo2S4 hollow microspheres as an advanced bifunctional electrocatalyst for aqueous metal/air batteries. *Catal. Sci. Technol.* 2016,*6* (2), 434-437, DOI: 10.1039/c5cy01656h.

[23.] Jia, N.; Liu, J.; Gao, Y.; Chen, P.; Chen, X.; An, Z.; Li, X.; Chen, Y. Graphene-Encapsulated Co9 S8 Nanoparticles on N,S-Codoped Carbon Nanotubes: An Efficient Bifunctional Oxygen Electrocatalyst. *ChemSusChem* 2019,*12* (14), 3390-3400, DOI: 10.1002/cssc.201900383.